BMC Biology

RESEARCH ARTICLE

Open Access

ARv7 promotes the escape of prostate cancer cells from androgen deprivation therapy-induced senescence by mediating the SKP2/p27 axis

Dian Zhuang[1†], Jinsong Kang[1†], Haoge Luo[2], Yu Tian[1], Xiaoping Liu[1] and Chen Shao[3*]

Abstract

Background Androgen deprivation therapy (ADT) induces cellular senescence and tumor stasis, thus serving as the standard treatment for prostate cancer (PCa). However, continuous suppression of canonical androgen receptor signaling actually leads to the switch from androgen-responsive growth to androgen-independent growth, contributing to "escape" from this ADT-induced senescence (AIS) and, subsequently, the development of castration-resistant prostate cancer (CRPC). Unfortunately, the mechanism underlying this phenomenon remains elusive.

Results In this study, we demonstrated that androgen receptor splicing variant 7 (ARv7), a dominant factor mediating abnormal AR signaling and ADT resistance, is closely associated with outgrowth from AIS of PCa cells. Mechanistically, ARv7 binds to the promoter of *SKP2*, activating its transcription, and then promotes the proteasomal degradation of the cell cycle regulator p27 and G1/S transition. In addition, we applied bioinformatic and in vitro analyses to show that SKP2 expression level is dramatically inhibited upon ADT, but its reactivation is one key step during the establishment of CRPC. Finally, we also demonstrated that SKP2 inhibitor treatment can significantly inhibit the growth of androgen-independent cell lines and enhance the efficacy of ADT.

Conclusions Our work reveals a novel role of ARv7 in regulating AIS and suggests that targeting the ARv7/SKP2/p27 axis could be a potential strategy to delay disease progression to the CRPC state during prolonged ADT.

Keywords Androgen deprivation therapy, Androgen independency, Senescence escape, ARv7, SKP2, p27

Background

Prostate cancer (PCa) is the most frequently diagnosed malignancy in men worldwide and is a major cause of cancer-related death, especially in Western countries [1]. Since ligand-dependent androgen receptor (AR) signaling plays a crucial role in the growth and progression of PCa, physicians and scientists have made substantial efforts to inhibit its hyperactivation [2]. Accordingly, androgen deprivation therapy (ADT) is the standard treatment option for both locally advanced and metastatic prostate cancer [3]. However, although ADT initially leads to tumor regression or stasis, entering a lethal castration-resistant state is almost inevitable for most

†Dian Zhuang and Jinsong Kang contributed equally to this work.

*Correspondence:
Chen Shao
shaochen@jlu.edu.cn
[1] Department of Pathophysiology, College of Basic Medical Sciences, Jilin University, Changchun 130021, China
[2] Department of Immunology, College of Basic Medical Sciences, Jilin University, Changchun 130021, China
[3] Department of Biochemistry & Molecular Biology, College of Basic Medical Sciences, Jilin University, Changchun 130021, China

PCa patients [4]. Thus, understanding how PCa cells switch from androgen-responsive growth to androgen-independent growth is of great importance for developing novel therapeutic strategies to delay progression to castration-resistant prostate cancer (CRPC) and improve the overall treatment outcomes of PCa patients.

Although ADT markedly restricts the level of androgen, abnormal activation of the AR pathway continues to play a dominant role in driving the progression of CRPC [5]. To date, numerous mechanisms have been proposed to contribute to the sustained activation of AR signaling, including overexpression of the AR gene or its coregulators, AR mutation, stimulation by oncogenic pathways, and the emergence of AR splicing variants (ARvs) [6, 7]. Of note, the expression of ARvs has drawn extensive attention as most ARvs lack the ligand binding domain but retain the DNA binding domain, enabling them to transcriptionally activate canonical AR-downstream events in the absence of androgen [8]. Among all the identified ARvs, ARv7 (also known as AR3) is the most studied and abundant form [9]. Accumulating evidence has highlighted the role of ARv7 in ADT resistance. For instance, ARv7 expression is induced in CRPC compared to hormone-naïve PCa, and depletion of ARv7 can dramatically inhibit androgen-independent growth of PCa cells and human xenografts [10]. Furthermore, ARv7 also strongly correlates with resistance to FDA-approved, second-generation AR inhibitors such as enzalutamide and abiraterone [11]. In recent years, many transcriptome-based studies have revealed that ARv7 not only recapitulates AR's typical functions but also mediates a unique gene expression program, which is likely vital for CRPC progression [12–14]. Unfortunately, most AR inhibitors target androgen binding or androgen synthesis, and there is no effective and specific inhibitor of ARv7 available in the clinic. Hence, understanding the detailed downstream events mediated by ARv7 will be helpful to specifically target the abnormal activation of AR signaling and improve the efficacy of ADT.

ADT does not efficiently eliminate androgen-responsive PCa cells but instead induces growth arrest in the majority of the subpopulation. Several recent studies have demonstrated that ADT induces cellular senescence marked by upregulation of senescence-associated-beta-galactosidase (SA-β-gal) and robust G0/G1 cell cycle arrest, offering a reasonable explanation for the initial tumor-suppressive function of ADT observed in the clinic [15, 16]. In general, senescence can be mediated through multiple signaling pathways, such as the well-defined p53-$p21^{Cip1/Waf}$ pathway and $p16^{INK4a-RB}$ pathway, which can either interact with each other or act independently to block cell proliferation [17]. Of note, the transition from G0/G1 phase to S phase is also tightly controlled by another cyclin-dependent kinase inhibitor, p27 (Kip1). Specifically, p27 inhibits the cyclin E/Cdk2 complex and activates the G1 restriction point [18]. Ewald et al. demonstrated that ADT dramatically increased the expression of p27 in both the LNCaP cell line and the LuCaP xenograft model [15]. Moreover, induction of p27 and suppression of its proteasomal degradation was shown to induce robust growth inhibition in PCa cells [19]. Ambiguously, Kokontis et al. reported that androgen treatment can suppresses the proliferation of PCa cells via inducing p27 expression [20]. In contrast, the downregulation of p27 disrupts proper control over the transition from G1 to S phase and leads to uncontrolled cell proliferation, which is closely related to the progression of several cancers, including PCa [21, 22]. However, how p27-mediated growth arrest is specifically overridden during prolonged ADT remains unclear.

It is well-established that those treatment-induced senescent cells are still metabolically active and may alter the tumor microenvironment to facilitate tumor progression, known as the senescence-associated secretory phenotype (SASP) [23]. In addition, ADT-induced senescence (AIS) seems reversible as cells can quickly resume proliferation upon restoration of androgen levels [24]. More importantly, the outgrowth of androgen-refractory progeny cells was observed after continuous exposure to an androgen-depleting environment, suggesting that a small population of the cells can even spontaneously escape AIS without being rejuvenated by androgen [24, 25]. Therefore, the cell fate after AIS determines the therapy response for PCa to a large extent. Strikingly, Carpenter et al. demonstrated that cells that escaped from AIS displayed increased expression of constitutively active ARvs [24]. However, whether and how ARvs affect AIS has not been investigated before. ARv7, but not its parental AR, was positively correlated with the level of several crucial cell cycle genes [12, 26]. In addition, our previous works have identified the role of ARv7 in regulating cell cycle checkpoint [27]. Hence, these findings motivate us to speculate that ARv7 may be also involved in the regulation of AIS.

In this study, we investigated the role of ARv7 in AIS and explored the mechanism by which ARv7 affects this specific cell cycle arrest. As a result, we provided data to show that ARv7 promotes the escape of PCa cells from AIS in an S phase kinase-associated protein 2 (SKP2)/p27-dependent manner. Mechanistically, ARv7 binds to the promoter of *SKP2*, activating its transcription, and then promotes the proteasomal degradation of p27 and subsequent G1/S transition. Of note, an outgrowth from AIS is also associated with increased expression of ARv7 and SKP2, and SKP2 inhibitor treatment can significantly inhibit the growth of androgen-independent cell lines.

Moreover, treatment with a low-dose SKP2 inhibitor also shows strong synergy with ADT in blocking the proliferation of androgen-independent PCa cells. In summary, our work unravels a novel role of ARv7 in AIS and suggests that targeting the ARv7/SKP2/p27 axis could be a potential strategy to delay disease progression to the CRPC state during ADT.

Results

ADT induces cellular senescence marked by robust p27 activation

In order to mimic the effect of ADT in vitro, we exposed the androgen-sensitive PCa cell line LNCaP to enzalutamide treatment or charcoal-stripped serum (CSS)-supplemented medium. Consistent with previous findings, both treatment with enzalutamide and CSS medium induced obvious cellular senescence in LNCaP cells as shown by the senescence-associated-β-galactosidase (SA-β-gal) activity assay (Fig. 1A and B). Moreover, strong G0/G1 cell cycle arrest was detected when we treated LNCaP cells with CSS medium and enzalutamide (Fig. 1C). In addition, we performed 5-ethynyl-2′-deoxyuridine (EdU) assays to further confirm that LNCaP cells treated with enzalutamide and CSS medium displayed significantly lower DNA replication activity than control cells, indicating that they failed to efficiently go through the G1/S transition (Fig. 1D and E). Of note, the Annexin V/PI staining data showed that no obvious apoptosis was detected using these two models, suggesting that ADT suppresses the cell viability of androgen-sensitive PCa cells in an apoptosis-independent manner (Fig. 1F). Next, to determine the possible senescence-associated pathways affected in our models, we examined the protein level changes in several cell cycle regulators that were previously demonstrated to be crucial for senescence induction. As the data presented in Fig. 1G, p21 levels were not affected in either model while p53 and p16 levels were increased in enzalutamide-treated cells but were not changed in cells treated with CSS medium. Strikingly, p27 levels were significantly increased in both models. Taken together, the data presented above suggest that ADT induces cellular senescence marked by robust p27 activation.

ARv7 promotes the escape of PCa cells from AIS

We next sought to determine whether ARv7 affects AIS by modifying ARv7 levels in PCa cells using lentivirus. First, we overexpressed ARv7 in LNCaP cells which normally express undetectable levels of endogenous ARv7. As shown in Fig. 2A and B, ARv7 overexpression (OE) significantly reduced the percentage of β-gal-positive cells after treatment with CSS medium and enzalutamide. Consistently, OE of ARv7 increased the percentage of EdU-positive cells after ADT-mimicking treatments (Fig. 2C and D). On the other hand, ENZ treatment hardly induced obvious senescence or growth arrest in ARv7-expressing, androgen-independent 22Rv1 cells, as shown by β-gal and EdU assays. However, when treated with ENZ, cells with ARv7 depletion displayed more senescent and fewer EdU-positive cells, indicating that ARv7 knockdown (KD) enhanced AIS in androgen-insensitive cells. Importantly, the ADT-resistant phenotypes can be rescued by expressing GFP tagged, recombinant ARv7 (Fig. 2E and F). As we speculated that p27 might be a crucial cell cycle regulator determining AIS [28], we next examined whether ARv7 affects the level of p27 during ADT. ARv7 OE weakened, while ARv7 KD enhanced, the stimulatory effect of ADT on p27 in LNCaP and 22Rv1 cells, respectively. Also, expression of exogenous GFP-ARv7 rescued the inhibitory effect on p27 induction in ARv7-depleting 22Rv1 cells (Fig. 2G and H). These data above suggest that ARv7 is specifically involved in the regulation of AIS and p27. Since p27 is primarily regulated at the posttranslational level and proteasomal degradation is one major way to decrease its protein level, we next focused on determining whether ARv7 affects this process. As shown in the cycloheximide (CHX) chase assay in Fig. 2I, OE of ARv7 accelerated, while KD of ARv7 slowed the degradation speed of ARv7 in LNCaP and 22Rv1 cells, respectively. Moreover, ARv7 OE also enhanced the polyubiquitination level of p27, further demonstrating that ARv7 promotes the proteasomal degradation of p27 during the G1/S transition (Fig. 2J). In sum, these data support that ARv7 promotes the escape of PCa cells from AIS.

Outgrowth from AIS is associated with increased levels of ARv7 and decreased levels of p27

Spontaneous escape from AIS during sustained androgen-depleting conditions finally contributes to androgen-independent growth of CRPC cells. Thus, we next designed experiments to further explore this process. First, we cultured LNCaP cells in CSS medium for different times and followed their growth properties as well as protein level changes during this long-term androgen-deprivation condition. As shown in Fig. 3A, compared with cells treated with CSS medium for 7 days, cells that underwent 65 days of CSS medium treatment exhibited significantly fewer senescent cells, suggesting that these cells started to escape from AIS and lose their senescence markers. Remarkably, we found that cells with longer exposure to androgen-depleting conditions expressed higher levels of ARv7 and anti-apoptotic protein Bcl-2 but lower levels of p27 (Fig. 3B). After culturing LNCaP cells in CSS medium for over 5 months, we successfully established

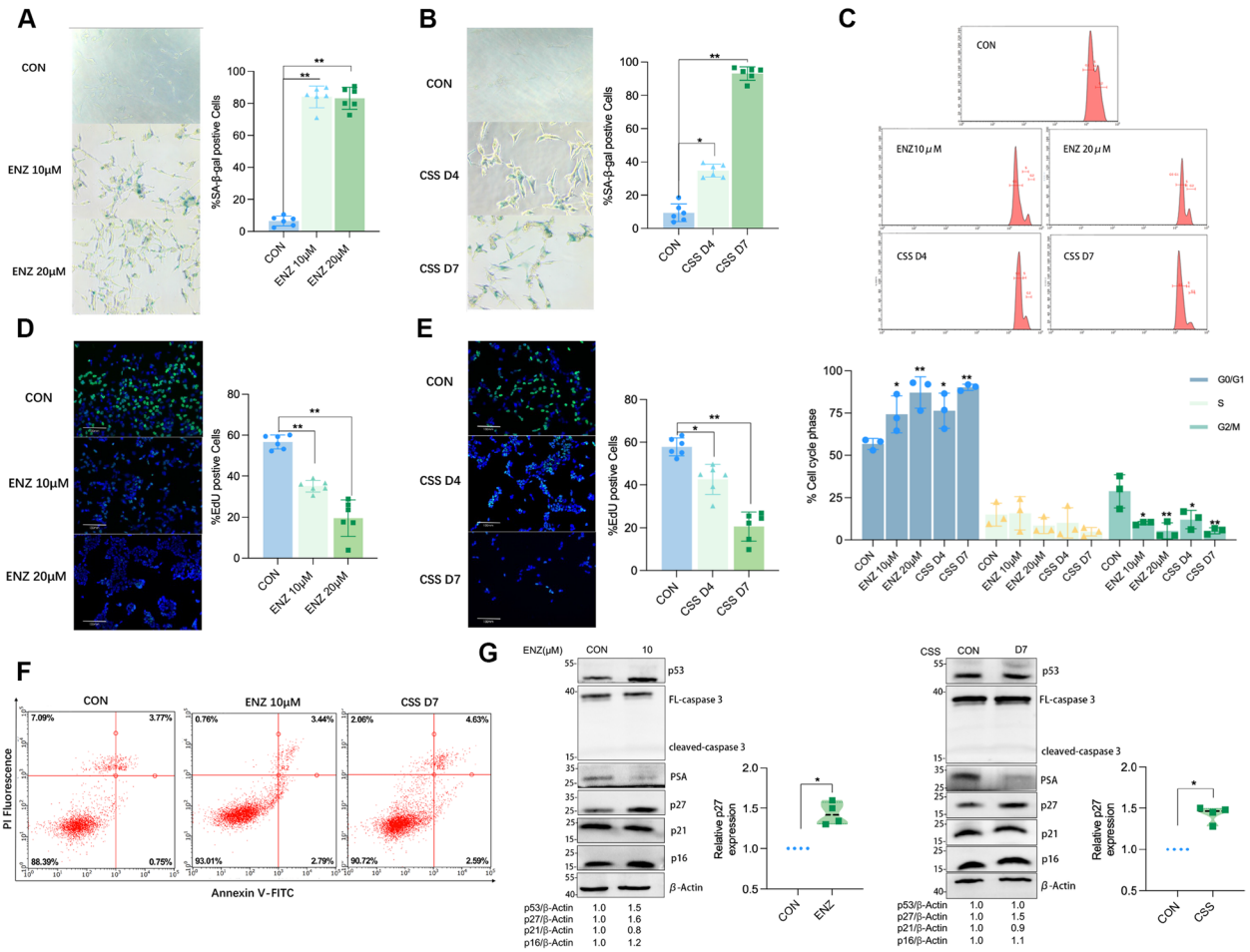

Fig. 1 ADT induces cellular senescence marked by robust p27 activation. **A** LNCaP cells were treated with DMSO control or different concentrations of enzalutamide for 72 h as indicated, and then the cells were subjected to an SA-β-gal activity assay to quantify the SA-β-gal-positive cells. At least 50 cells were counted for each experimental group, $^{**}P < 0.01$. **B** LNCaP cells were treated with normal medium as control or charcoal-stripped serum (CSS)-supplemented medium for different times as indicated, and then the cells were subjected to an SA-β-gal activity assay, $^{*}P < 0.05$. **C** LNCaP cells with different treatments as indicated above were harvested for FACS analysis, data were repeated at least three times, and percentages of each cell cycle stage are shown as the mean ± SD. **D** and **E** LNCaP cells with different treatments as indicated above were subjected to EdU assays, then the EdU-positive cells were quantified to assess the activity of DNA replication, and at least 50 cells were counted for each field. **F** LNCaP cells were treated with 10 μM enzalutamide (72 h) or CSS medium (7 days) and harvested for Annexin V/PI staining. Annexin V-positive and double-positive cells were quantified as apoptotic cells, and at least three independent assays were performed for each experimental group. **G** LNCaP cells were treated with 10 μM enzalutamide (72 h) or CSS medium (7 days) and harvested for immunoblotting (IB) analysis; each IB was repeated for at least three times to perform the statistical analysis of the bands. Specifically, the expression levels of p27 were shown as bar graph

the LNCaP-AI (androgen-independent) cell line. Compared with their parental cells, LNCaP-AI cells were much more resistant to AIS, as illustrated by β-gal and EdU assays (Fig. 3C, D, and E). More importantly, LNCaP-AI cells showed sharply decreased p27 expression compared with parental cells, indicating that p27 was dramatically inhibited during AIS escape (Fig. 3F).

SKP2 is crucial for regulating p27 and AIS

ARv7 primarily exerts its oncogenic function as a constitutively active transcriptional factor. Thus, to investigate the mechanism by which ARv7 regulates cell cycle progression and AIS, we utilized our previous RNA-seq data using 22Rv1 cells and 22Rv1 cells with stable ARv7 depletion (GSE277204). Consistent with the analysis we performed in another PCa cell line [29], GSEA analysis revealed that the cell cycle-related gene signature was negatively enriched after ARv7 knockdown (Fig. 4A). In

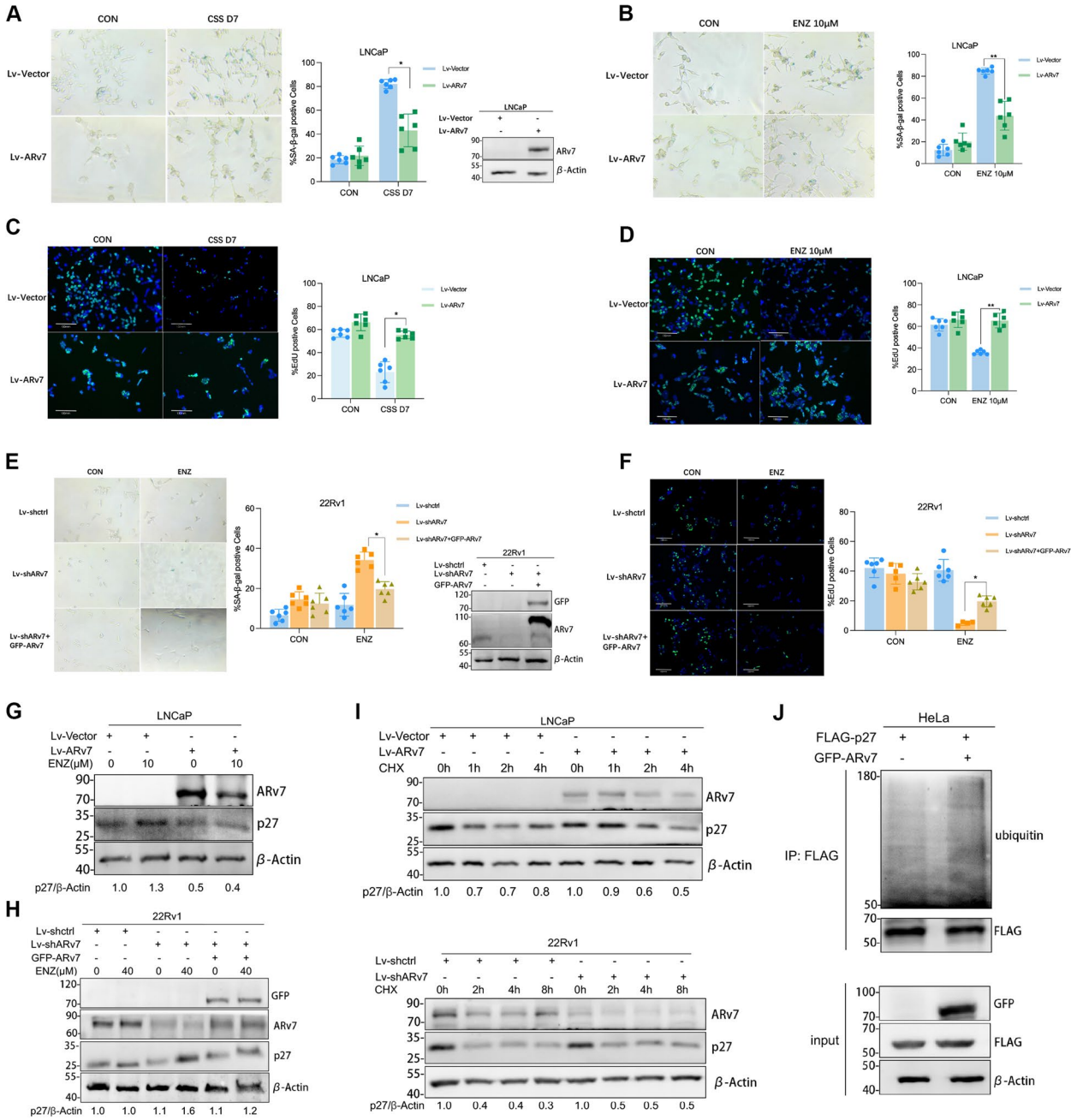

Fig. 2 ARv7 promotes the escape of PCa cells from AIS. **A** Left panel, stable virus-infected LNCaP cells (vector or ARv7 OE) were treated with normal medium or CSS medium for 7 days and then subjected SA-β-gal activity assays. Right panel, the expression levels of ARv7 in two cell lines were analyzed using IB. **B** Stable virus-infected LNCaP cells (vector or ARv7 OE) were treated with DMSO control or 10 μM enzalutamide for 72 h and then subjected to an SA-β-gal activity assay. **C** Stable virus-infected LNCaP cells (vector or ARv7 OE) were treated with normal medium or CSS medium for 7 days and then subjected to EdU assay. **D** Stable virus-infected LNCaP cells (vector or ARv7 OE) were treated with DMSO or 10 μM enzalutamide for 72 h and then subjected to EdU assay. **E** Left panel, stable virus-infected 22Rv1 cells (shctrl or shARv7 or shARv7 transfected with GFP-ARv7) were treated with DMSO control or 40 μM enzalutamide for 72 h and then subjected to SA-β-gal activity assays. Right panel, the expression levels of endogenous and exogenous ARv7 in three groups were analyzed using IB. **F** Stable virus-infected 22Rv1 cells (shctrl or shARv7 or shARv7 transfected with GFP-ARv7) were treated with DMSO or 40 μM enzalutamide for 72 h and then subjected to EdU assays. **G** Stable virus-infected LNCaP cells (vector or ARv7 OE) were treated with DMSO or 10 μM enzalutamide for 72 h and then subjected to IB. **H** Stable virus-infected 22Rv1 cells (shctrl or shARv7) were transfected with empty vector or GFP-ARv7 plasmid for 24 h, treated with 40 μM enzalutamide for another 48 h, and then subjected to IB. **I** Upper panel, stable virus-infected LNCaP cells (vector or ARv7 OE) were treated with 10 μg/ml CHX for different times as indicated and then harvested for IB. Lower panel, stable virus-infected 22Rv1 cells (shctrl or shARv7) were treated with 10 μg/ml CHX for different times as indicated and then harvested for IB. **J** HeLa cells were transfected with the indicated plasmids for 48 h, treated with 10 μM MG132 for an additional 6 h, and then harvested for IB and IP using the antibodies indicated in the figure

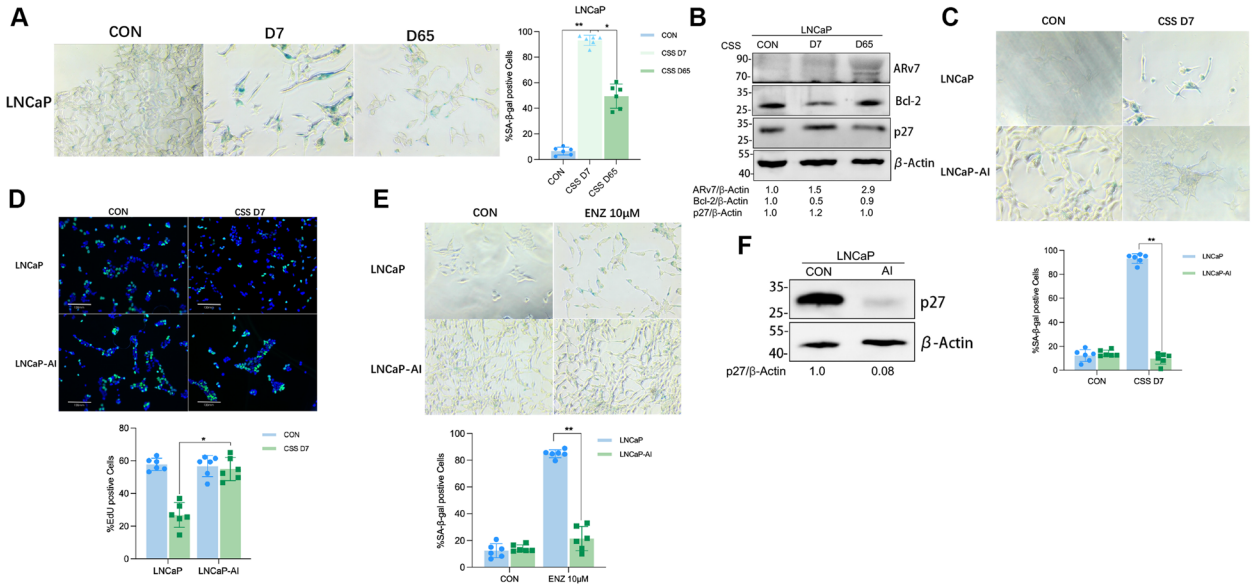

Fig. 3 Outgrowth from AIS is associated with increased levels of ARv7 and decreased levels of p27. **A** LNCaP cells were cultured in CSS medium for different times as indicated and harvested for the SA-β-gal activity assay. **B** LNCaP cells were cultured in CSS medium for different times and then harvested for IB. **C** LNCaP and LNCaP-AI cells were treated with normal medium or CSS medium for 7 days and then subjected to an SA-β-gal activity assay. **D** LNCaP and LNCaP-AI cells were treated with normal medium or CSS medium for 7 days and then subjected to EdU assay. **E** LNCaP and LNCaP-AI cells were treated with DMSO or 10 μM enzalutamide for 72 h and then subjected to an SA-β-gal activity assay. **F** Randomly growing LNCaP and LNCaP-AI cells were harvested for IB analysis against p27

support of our previous findings [27], most of the differentially expressed cell cycle-related genes were associated with the G2/M transition and mitotic regulation, as shown in the heat map data. Of note, the expression levels of several genes that regulate DNA replication (*ORC5/6*, *MCM5/6*, etc.) and G1/S transition (*CDC7*, *E2F2*, *SKP2*, etc.) were also repressed after ARv7 depletion (Fig. 4B). Among the genes mediating the G1/S transition, *SKP2* draws our attention as *SKP2* encodes an E3 ligase called S phase kinase-associated protein 2 (SKP2), which is crucial for mediating the G1/S transition by promoting p27 proteasomal degradation. Accordingly, we next decided to focus on understanding the regulation of SKP2 during AIS. As a result, we found that both the protein and mRNA levels of SKP2 were significantly decreased after ADT in LNCaP cells, which was consistent with senescence induction and p27 accumulation (Fig. 4C and D). However, long-term exposure to CSS medium resulted in restored expression of SKP2 (Fig. 4E). Moreover, compared with parental LNCaP cells, LNCaP-AI cells showed enhanced SKP2 expression levels, suggesting that reactivation of SKP2 plays an important role during the transition from androgen-sensitive growth to androgen-insensitive growth (Fig. 4F). To further confirm the role of SKP2 in AIS, we applied the SKP2-specific inhibitor C1 in the following experiments. First, treatment with SKP2 inhibitor (SKP2i) dramatically stabilized p27, as illustrated by CHX chase assays (Fig. 4G). In addition, as shown in Fig. 4H, I, and J, treatment with SKP2i induced senescence and G0/G1 growth arrest in LNCaP cells. Taken together, these data indicate that the E3 ligase SKP2 is crucial for regulating p27 levels and AIS.

ARv7 mediates AIS in an SKP2-dependent manner

To confirm whether SKP2 is a downstream target of ARv7 as indicated in the RNA-seq analysis, we used publicly available genomic binding profiles (GSE99378 and GSE94013). As a result, we were able to observe signal of ARv7 but not AR-FL enrichment at the promoter region of SKP2; UBE2C was also displayed as a known downstream gene of ARv7 (Fig. 5A). Moreover, we performed ChIP-qPCR assays employing a primer downstream of the SKP2 transcription starting site (TSS) to validate that ARv7 binds to the promoter of SKP2 (Fig. 5B). In addition, luciferase assay also suggested that ARv7 expression induced dramatic transcriptional activation (over tenfold changes) at SKP2 promotor (Fig. 5C). Consistent with the ChIP-qPCR and luciferase data, both the protein and mRNA levels of SKP2 were increased after ARv7 OE in LNCaP cells (Fig. 5D and F), while ARv7 depletion downregulated the protein and mRNA levels of SKP2 in 22Rv1 cells (Fig. 5E and G). Of note, the expression levels of AR-FL were not affected in both models. In addition,

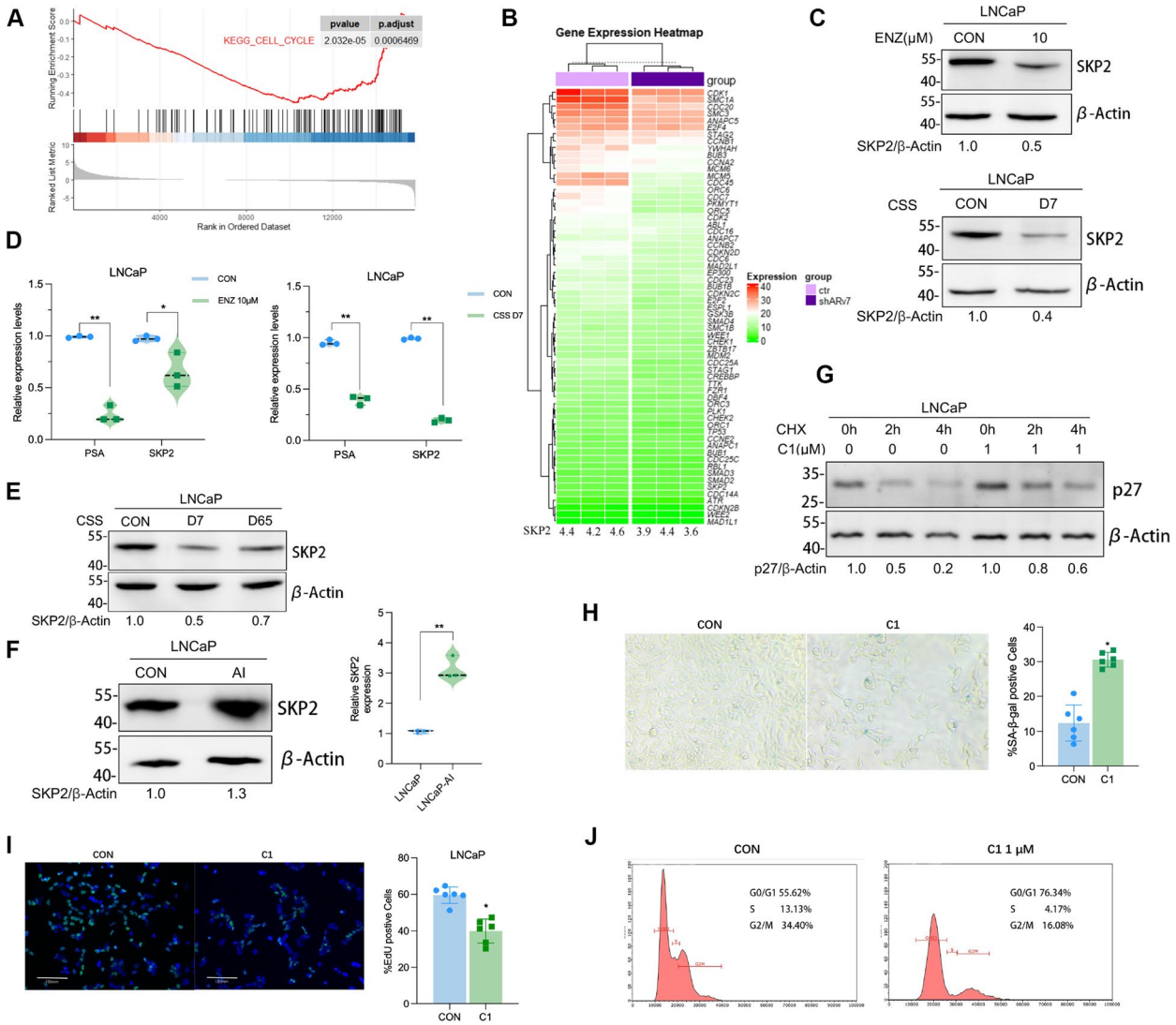

Fig. 4 SKP2 is crucial for regulating p27 and AIS. **A** GSEA analysis of RNA-seq data showing the negative enrichment of the cell-cycle gene signature in ARv7-depleted 22Rv1 cells. **B** Heat map analysis between two groups of 22Rv1 cells (shctrl or shARv7) shows where expression is high (red) or low (green) for each hallmark cell-cycle gene. **C** LNCaP cells were treated with 10 μM enzalutamide for 72 h or CSS medium for 7 days and then harvested for IB. **D** LNCaP cells were treated with 10 μM enzalutamide for 72 h or CSS medium for 7 days and then harvested for qRT-PCR analysis. Data represent the average of three independent experiments ± SD. PSA levels were also checked for measuring the efficacy of ADT-mimicking treatment. **E** LNCaP cells were cultured in CSS medium for different times and then harvested for IB using an antibody against SKP2. **F** LNCaP and LNCaP-AI cells were harvested for IB and qRT-PCR analysis. **G** LNCaP cells were pretreated w/o 1 μM SKP2 inhibitor C1 for 24 h and then cultured with 10 μg/ml CHX for different times as indicated before being harvested for IB. **H** LNCaP cells were treated with 1 μM SKP2 inhibitor C1 for 24 h and then harvested for the SA-β-gal activity assay. **I** LNCaP cells were treated with 1 μM SKP2 inhibitor C1 for 24 h and then harvested for EdU assay. **J** LNCaP cells were treated with 1 μM SKP2 inhibitor C1 for 24 h and then harvested for FACS analysis

we were able to observe the similar result in PC-3, which is an AR-null cell line, further demonstrating that ARv7 can regulate SKP2 independent of its parental AR-FL (Fig. 5H). Importantly, we found that treatment with SKP2i largely impaired the function of ARv7 in promoting the escape of LNCaP cells from AIS, as shown by the EdU assay, indicating that ARv7 mediates escape from AIS in a partially SKP2-dependent manner (Fig. 5I).

SKP2 activation correlates with ADT resistance and androgen-independent growth of PCa cells

Given the important role of SKP2 in regulating p27 levels and cell cycle progression, we speculated that SKP2 upregulation might be correlated with ADT resistance.

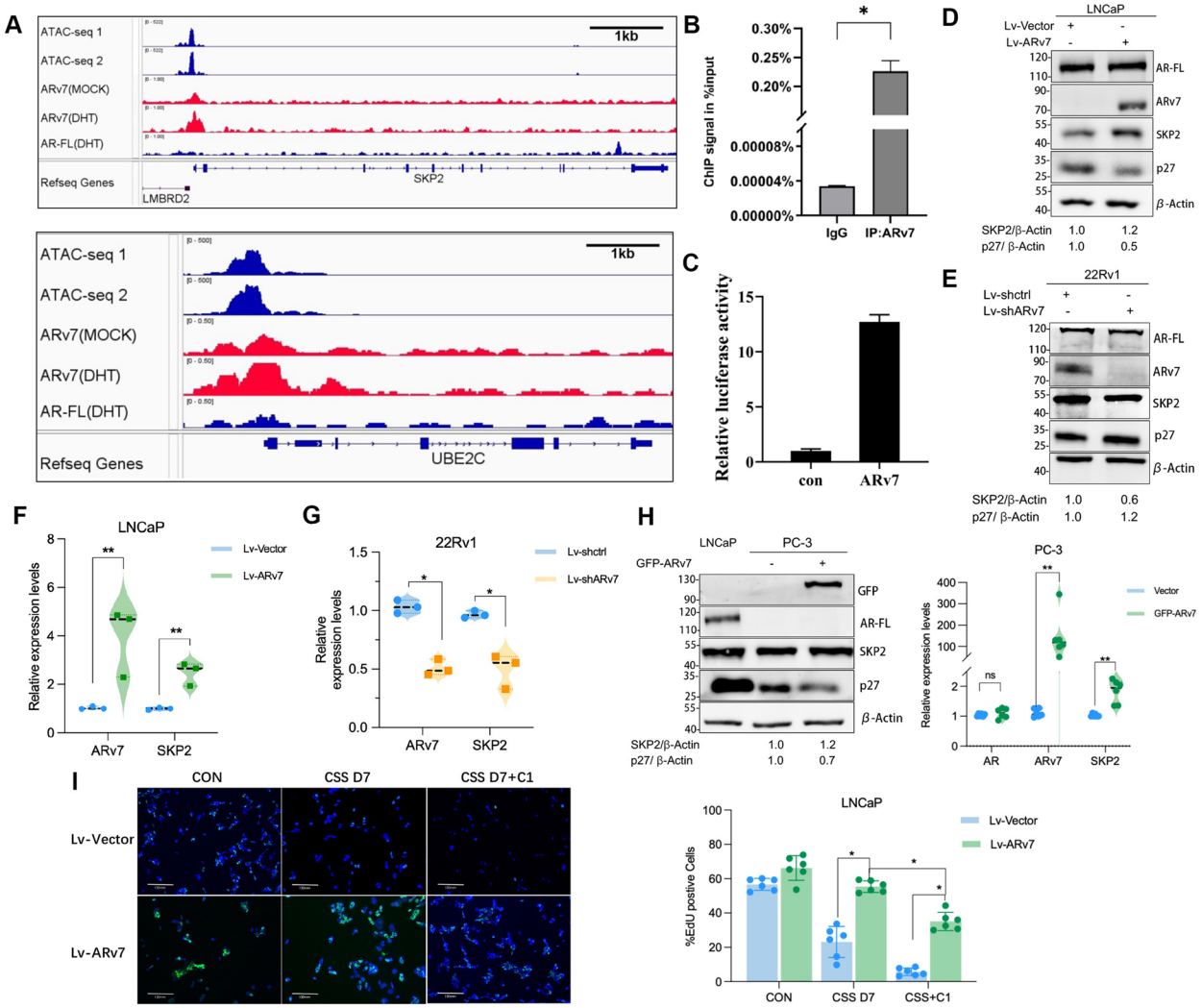

Fig. 5 ARv7 mediates AIS in an SKP2-dependent manner. **A** Integrative Genomics Viewer (IGV) image showing the enrichment for the indicated factor at *SKP2* and *UBE2C* in 22Rv1 cells, ATAC-seq data was applied to show the area of open chromatin. **B** ChIP-qPCR of ARv7 and IgG control at the promoter site in 22Rv1 cells. Data represent the average of three independent experiments ± SD. **C** HEK293T cells were co-transfected with SKP2 reporter plasmid, Renilla plasmid, and w/o GFP-ARv7 plasmid for 48 h, then cells were subjected to luciferase assay. Relative luciferase activity was calculated after normalized to Renilla luciferase unit. **D** Stable virus-infected LNCaP cells (vector or ARv7 OE) were harvested for IB. **E** Stable virus-infected 22Rv1 cells (shctrl or shARv7) were harvested for IB. **F** Stable virus-infected LNCaP cells (vector or ARv7 OE) were harvested for qRT-PCR analysis. **G** Stable virus-infected 22Rv1 cells (shctrl or shARv7) were harvested for qRT-PCR analysis. **H** Upper panel, PC-3 cells were transfected with empty vector or GFP-ARv7 for 48 h and harvested for IB; LNCaP cell lysate was analyzed together as a positive control for AR-FL expression. Lower panel, PC-3 cells were transfected with empty vector or GFP-ARv7 for 48 h and harvested for qRT-PCR analysis. **I** Stable virus-infected LNCaP cells (vector or ARv7 OE) were treated with normal medium or CSS medium for 7 days then treated w/o 1 μM SKP2 inhibitor C1 for another 24 h before being harvested for EdU assay

To validate this hypothesis, we utilized public datasets. By using the data from GDS3358, which performed a longitudinal analysis of gene expression in cultured LNCaP prostate cancer cells during 12 months of androgen deprivation, we revealed that SKP2 expression was sharply decreased initially upon androgen removal but started to be restored after 5 months of culturing and even showed increased expression after 11 months compared with the control group (Fig. 6A). These data are consistent with what we have shown in Fig. 3, further demonstrating that reactivation of SKP2 plays an important role during the switch from androgen-responsive growth to androgen-independent growth of PCa cells. In addition, we also analyzed the expression of SKP2 in a patient-based dataset (GSE35988) including benign prostate tissues ($n = 28$), localized prostate cancer ($n = 59$), and metastatic

castration-resistant prostate cancer (CRPC, $n=35$). As presented in Fig. 6B, SKP2 expression levels were relatively higher in the CRPC groups than in the benign prostate tissue group and the localized PCa group. Consistently, we obtained similar but more obvious results by analyzing GSE32269, which compared 22 primary PCa (hormone-dependent) versus 29 metastatic PCa (CRPC) samples (Fig. 6C). Based on those data, we next determined whether inhibition of SKP2 will efficiently inhibit the growth of androgen-independent PCa cells. As a result, SKP2i C1 treatment significantly repressed the viability of LNCaP-AI and 22Rv1 cells with IC_{50} values of 2.1 ± 0.1 μM and 500 ± 100 nM, respectively (Fig. 6D and E). Moreover, SKP2i also efficiently blocked the colony formation of both LNCaP-AI and 22Rv1 cells (Fig. 6F and G). Finally, SKP2i treatment was able to induce cellular senescence, cell cycle arrest, and p27 accumulation in both LNCaP-AI and 22Rv1 cells (Fig. 6H–M), suggesting that SKP2 inhibition was still efficient in those ADT-resistant cells.

SKP2 inhibitor exerts a synergistic effect with ADT in androgen-independent PCa cells

Since SKP2 plays a crucial role in promoting the escape of PCa cells from AIS downstream of ARv7, we proposed that targeting SKP2 activation could be an effective way to enhance the efficacy of ADT in ARv7-expressing, androgen-independent cells. To validate this hypothesis, we applied a low dose of SKP2i together with CSS medium treatment in androgen-insensitive PCa cells. As shown in Fig. 7A and B, neither CSS medium nor low-dose SKP2i treatment alone had an obvious effect in inhibiting colony formation of LNCaP-AI and 22Rv1 cells, whereas strong repression of cell growth was detected in the combination group. In addition, with a combination index equal to 0.512, SKP2i also showed a synergistic effect with enzalutamide in inhibiting the viability of LNCaP-AI cells (Fig. 7C). Consistently, SKP2i and enzalutamide also acted synergistically to inhibit colony formation of both LNCaP-AI and 22Rv1 cells (Fig. 7D and E). Overall, our work has proposed an ARv7/SKP2/p27 signaling pathway in mediating the efficacy of ADT in PCa cells (Fig. 7F).

Discussion

Cellular senescence is generally considered a stress-induced cell-cycle arrest that prevents the further expansion of malignant cells. However, some groups have claimed that therapy-induced senescence (TIS) may serve as an unfavorable response to anticancer therapies. Firstly, the SASP associated with TIS has been linked to an active paracrine fashion that contributes to the tumor-promoting immune microenvironment, epithelial-to-mesenchymal transition (EMT), and drug-resistance in adjacent cells [30, 31]. In addition, Milanovic et al. revealed that the induction of senescence in cancer cells markedly drives the expression of stem cell-associated genes. More importantly, a small proportion of those cells are able to break through the cell-cycle barrier and possess a greater capacity to facilitate tumor growth than cells that did not undergo a senescent state [32]. Clearly, the findings listed above challenge the traditional definition of senescence, which is usually considered irreversible and beneficial for cancer treatment. Regarding the "side effects" of the senescent state during cancer therapy, selective elimination of senescent cancer cells or blocking spontaneous escape from the arrested cell cycle will be beneficial for improving the overall treatment outcomes.

ADT barely induces apoptosis in androgen-dependent PCa cells but leads to senescence-like growth arrest both in vitro and in vivo. However, similar to the results observed in other models, escape of senescent PCa cells during prolonged ADT is frequently detected and contributes to the development of castration resistance [33]. For instance, androgen deprivation in LNCaP cells induces robust senescence, but the LNCaP-AI cell line

(See figure on next page.)

Fig. 6 SKP2 activation correlates with ADT resistance and androgen-independent growth of PCa cells. **A** Analysis of the relative expression levels of *SKP2* using the curated data from GDS3358. Each red column represents the expression measurement extracted from the VALUE column of one original submitter-supplied sample record. The blue square represents the rank order of expression measurements. **B** The expression of *SKP2* and that in comparison among benign prostate tissues, localized prostate cancer tissues and metastatic castration-resistant prostate cancer tissues in GSE35988. **C** The expression of *SKP2* and that in comparison between primary PCa tissues and mCRPC tissues in GSE32269. **D** LNCaP-AI cells were treated with different concentrations of SKP2i as indicated for 72 h and harvested for the MTT assay. **E** 22Rv1 cells were treated with different concentrations of SKP2i as indicated for 72 h and harvested for the MTT assay. **F** LNCaP-AI cells were seeded in 6-well plates (4000 cells per well) and treated with 200 nM SKP2i C1 for 14 days. The medium was refreshed every 3 days, and finally, the cells were fixed and stained with crystal violet followed by quantification of the clones. **G** 22Rv1 cells were seeded in 6-well plates (4000 cells per well) and treated with 50 nM SKP2i C1 for 14 days. The medium was refreshed every 3 days, and finally, the cells were subjected to a colony formation assay. **H** LNCaP-AI cells were treated with DMSO or 5 μM SKP2i C1 for 24 h and then subjected to SA-β-gal activity assays. **I** LNCaP-AI cells were treated with DMSO or 5 μM SKP2i C1 for 24 h and then subjected to EdU assays. **J** LNCaP-AI cells were treated with DMSO or 5 μM SKP2i C1 for 24 h and then harvested for IB. **K** 22Rv1 cells were treated with DMSO or 5 μM SKP2i C1 for 24 h and then subjected to SA-β-gal activity assays. **L** 22Rv1 cells were treated with DMSO or 5 μM SKP2i C1 for 24 h and then subjected to EdU assays. **M** 22Rv1 cells were treated with DMSO or 5 μM SKP2i C1 for 24 h and then harvested for IB

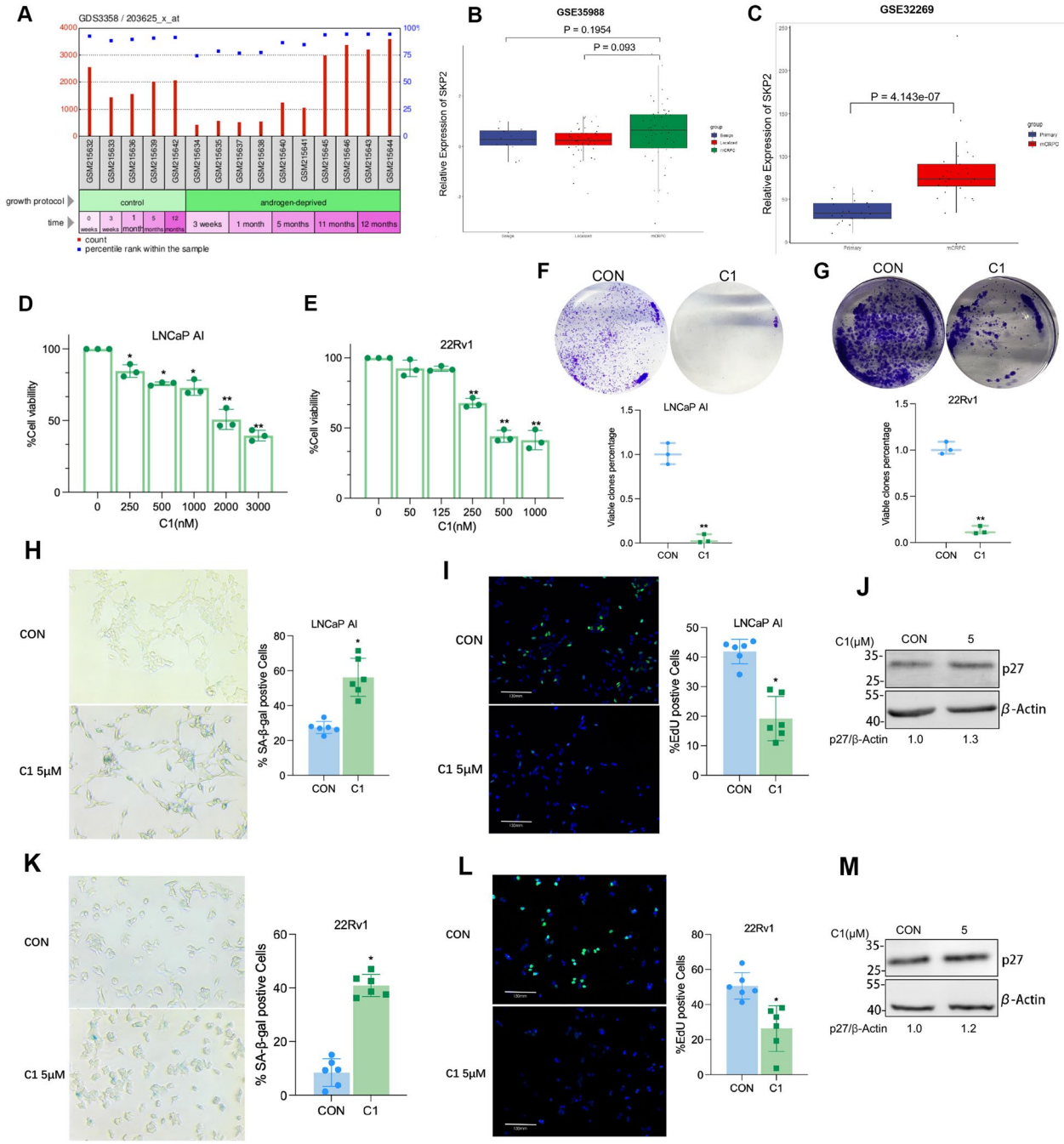

Fig. 6 (See legend on previous page.)

is established by long-term culture in CSS medium and then exhibits androgen-independent growth properties and a more aggressive phenotype [34]. As other studies have reported, these subpopulations even exhibit increased expression of the apoptosis-resistant marker survivin and prostatic basal stem cell marker TAp63 [28]. However, how PCa cells overcome this specific growth arrest and switch to androgen-independent growth is poorly understood. Remarkably, the outgrowth from senescence was associated with increased expression of constitutively active ARvs in a mouse PCa cell line [24]. Considering the critical role of ARvs in mediating androgen-independent growth and ADT resistance, this finding suggests a potential link between ARvs and the fate of PCa cells after AIS. In this study, we specifically focused on investigating the

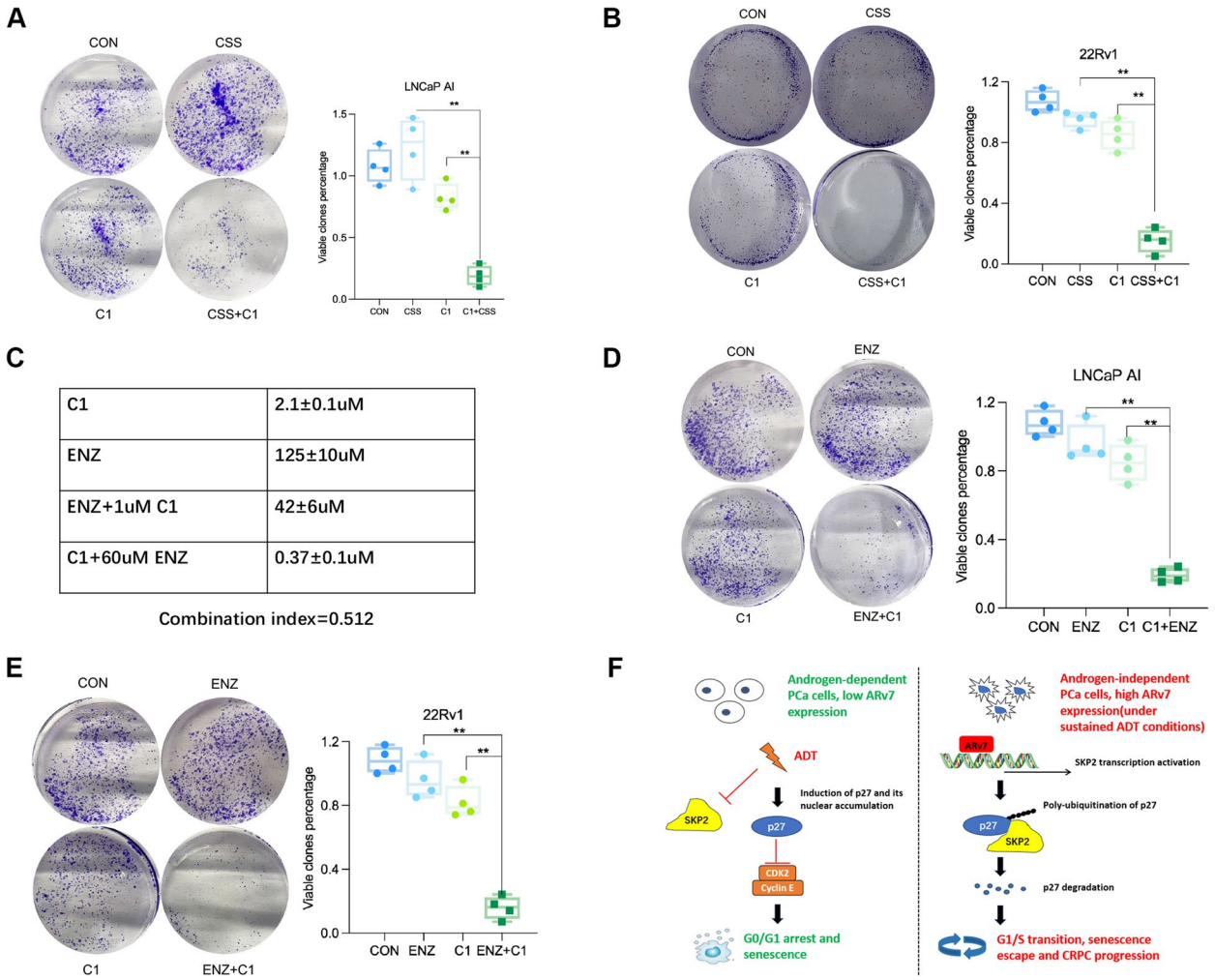

Fig. 7 SKP2 inhibitor exerts a synergistic effect with ADT in androgen-independent PCa cells. **A** LNCaP-AI cells were seeded in 6-well plates (2000 cells per well), treated with CSS medium, 50 nM SKP2i C1, or both for 14 days, and harvested for colony formation assays. **B** 22Rv1 cells were seeded in 6-well plates (2000 cells per well), treated with CSS medium, 20 nM SKP2i C1, or both for 14 days, and harvested for colony formation assays. **C** IC_{50} values of SKP2i C1 and enzalutamide in LNCaP-AI cells. The combination index was calculated and displayed below the table. **D** LNCaP-AI cells were seeded in 6-well plates (2000 cells per well), treated with 400 nM enzalutamide, 50 nM SKP2i C1, or both for 14 days, and harvested for colony formation assays. **E** 22Rv1 cells were seeded in 6-well plates (2000 cells per well), treated with 800 nM enzalutamide, 20 nM SKP2i C1, or both for 14 days, and harvested for colony formation assays. **F** The proposed model for this study

role of ARv7 using human PCa cell lines to determine the possible mechanism by which ARv7 contributes to escape from AIS. As a result, we found that ARv7 significantly promotes the escape of PCa cells from AIS, which could be a prerequisite for its function during androgen-independent growth. Previously, our group identified the novel role of ARv7 in regulating mitotic exit [27]. This time, we are also the first to propose the key function of ARv7 in the G1/S transition, especially under the condition of AIS. Combined, our findings further validate the previous observation that ARv7 mediates a distinct transcriptional network enriched for cell cycle-related genes from its parental AR [12].

Several previous studies have examined the possible molecular mechanisms for AIS. Burton et al. suggested that AIS is achieved through ROS-induced DNA damage and the $p16^{INK4a}$ pathway rather than the p53/p21 pathway [25]. However, p27 seems to play a dominant role in ADT-mediated cell cycle arrest in another two studies [15, 35]. In addition to those cell cycle regulators-based studies, upregulation of C/EBPβ has also been demonstrated to be critical for the complete maintenance of AIS [36]. Based on our results, we confirmed that p27 but not p21 was robustly induced after ADT, while p16 expression was only induced after enzalutamide treatment but not in the CSS medium. Unfortunately, we could not

further explain this discrepancy between these two typical ADT-mimicking models. Thus, in the following of our work, we focused on the regulation of p27 during ADT.

Posttranslational regulation primarily determines the function of p27, mediating its subcellular localization and inhibitory effect on the cell cycle. When cells enter the S phase, phosphorylation of p27 at T187 by the cyclin E/CDK2 complex allows it to be degraded by the SCF protein complex in the nucleus [37]. Numerous pieces of evidence have supported that the F-box protein SKP2 is a bona fide E3 ligase for p27, inducing K48-linked ubiquitination of p27 and its proteasomal degradation [38]. Of note, high SKP2 expression and its hyperactivation are reported in many cancers. More specifically, ectopic expression of SKP2 can even reverse the senescent state, releasing cells from this so-called permanent growth arrest [39]. Thus, inhibition of SKP2 may enhance the efficacy of cancer treatment by preventing escape from TIS. Our study shows that ARv7 directly binds to the promoter of *SKP2* and promotes its transcription, through which ARv7 accelerates the degradation of p27 and overcomes the G0/G1 arrest induced by ADT. Consistent with our data, Cai et al. have also demonstrated that *SKP2* is one of the top hit genes uniquely upregulated by ARv7 but not AR using a cistrome profiling approach [26].

To our knowledge, some previous studies have already indicated the potential links among p27, SKP2, and the AR pathway. First, Fang et al. found that activation of AR signaling promotes the degradation of p27 in a mTORC2/AKT-dependent manner [40]. Moreover, SKP2 was demonstrated to be downregulated after ADT [35]. To make things more complicated, SKP2 was also reported to be an E3 ligase for AR [41]. More recently, one study reported that SKP2 acetylation by p300 contributes to the progression of CRPC, and this signaling can be further stimulated by androgen [42]. However, the regulation of SKP2 and p27 during the establishment of androgen independency has not been investigated before. Currently, our findings suggest that constitutively active ARv7 can serve as a critical upstream regulator of SKP2 activation and p27 degradation, offering a novel mechanism for how PCa cells overcome AIS under long-term androgen-depleting conditions. Moreover, we also demonstrated that reactivation of SKP2 may serve as a critical step during the progression of CRPC by analyzing both cell- and patient-based datasets (Fig. 6). Accordingly, we designed experiments to show that applying an inhibitor of SKP2 can significantly inhibit the growth of ARv7-expressing, androgen-independent cell lines and enhance the efficacy of ADT. Based on this finding, we may continue to investigate cell fate after being previously senescent, which may provide further insight into the specific role of ARv7 in mediating therapy resistance and cell plasticity.

It is challenging to delineate the roles of ARv7 and the AR-FL in transcriptional regulation, especially during the condition of CRPC or continuous ADT for the following reasons. Firstly, ARvs are constantly associated with AR-FL without any clinical sample detected being solely ARvs-positive [43]. In addition, ARv7 can either function independently or form heterodimers with AR-FL [44]. More importantly, AR-FL mediates a distinct transcriptional program that is enriched for cell cycle events and DNA damage repair under the conditions of androgen depleting [45]. And this unique transcriptional network displays unexpectedly high consistency with what we and others have observed in ARv7-based RNA-sequencing results [29, 46]. In sum, these findings suggest that ARv7 may cooperate with AR-FL in the reprogramming of AR signaling under continuous ADT situation. Although we provided data to demonstrate that the overall effect in this manuscript is mainly attributed to ARv7, future experiments are required to better distinguish the role between AR-FL and ARv7 in AIS regulation.

Conclusions

Overall, our study identifies an ARv7/SKP2/p27 signaling pathway in mediating AIS. Although we cannot efficiently prevent the emergence of ARv7 or disrupt its activity, applying SKP2-specific inhibitors together with ADT may be beneficial for delaying the progression of CRPC.

Methods

Chemicals

SKP2 inhibitor C1, cycloheximide, MG132, and enzalutamide were purchased from TargetMol (Boston, MA, USA), while puromycin was purchased from MedChemExpress (Monmouth Junction, NJ, USA).

Cell culture, plasmid transfection, and virus infection

C4-2, PC-3, and 22Rv1 cells were originally purchased from ATCC, and LNCaP cells were kindly provided by StemCell Bank, Chinese Academy of Sciences. LNCaP, C4-2, PC-3, and 22Rv1 cells were cultured in RPMI 1640 medium (Gibco Life Technologies, Carlsbad, CA, USA) supplemented with 10% fetal bovine serum, 100 U/ml penicillin, and 100 U/ml streptomycin in 5% CO2 at 37 °C. LNCaP-AI cells were established by culturing LNCaP cells in RPMI 1640 medium containing charcoal-stripped serum (CLARK BIOSCIENCE) for over 5 months. For plasmid transfection, EGFP-ARv7 was obtained from Addgene and transfected into cells using lipofectamine 2000 (ThermoFisher). For lentivirus infection, cells stably

expressing ARv7 or cells with ARv7 depletion were generated as previously described [27].

Immunoblotting and immunoprecipitation

Cell lysates were prepared using RIPA buffer (Boston BioProducts, Ashland, MA, USA) supplemented with protease inhibitors (Sigma) and phosphatase inhibitors (Active Motif, Carlsbad, CA, USA). For immunoprecipitation experiments, cell lysates were incubated with the desired antibodies in Tris buffered saline buffer at 4 °C overnight, and then protein G agarose (Beyotime Biotechnology, Shanghai, China) was added to each sample for another 2 h incubation, followed by five washes with PBS solution and boiling for IB. Antibodies against ARv7 (ab198394) were obtained from Abcam, antibodies against SKP2 (2652), p27 (3686), p21 (2947), p16 (18,769), AR (54,653), and PSA (5365) were purchased from Cell Signaling Technology (Danvers, MA, USA), and antibodies against GFP (sc-9996), p53 (sc-126), and ubiquitin (sc-8017) were obtained from Santa Cruz. Proteintech (Chicago, IL, USA) is the provider of antibodies against caspase 3, cleaved-caspase 3, β-actin, Bcl-2, and FLAG.

Cell viability assay

Cells were seeded in 96-well plates and treated with the indicated drugs or DMSO as a control for 72 h. Then, the medium was removed, and 0.5 mg/ml MTT was added for 4 h. Formazan crystals were dissolved in 150 μl of DMSO, and the absorbance was measured at a wavelength of 490 nm. The combination index of enzalutamide and SKP2i was measured using the following equation: combination index $= (Am)_{50}/(As)_{50} + (Bm)_{50}/(Bs)_{50}$, where $(Am)_{50}$ is the IC_{50} of enzalutamide in the combination with half of the concentration of the SKP2i IC_{50}, $(As)_{50}$ is the concentration of enzalutamide that will produce the identical level of effect alone, $(Bm)_{50}$ is the IC_{50} of SKP2i in the combination with half of the concentration of the enzalutamide IC_{50}, and $(Bs)_{50}$ is the IC_{50} of SKP2i after a single administration. Combination indices of >1, 1, and <1 indicate antagonism, an additive effect, and synergy, respectively.

Flow cytometry

Cells were seeded in 6-well plates. After exposure to different treatments, cells were collected and PI staining was performed according to the manufacturer's instructions. Then, samples were analyzed by Accuri C6 Flow Cytometry (BD Biosciences).

Quantitative PCR

Total RNA was extracted from cells using TRIzol (Invitrogen) according to the manufacturer's protocol. Briefly, cDNA was synthesized using 0.5 μg of total RNA and a SuperScript preamplification system (Promega, Madison, WI). The primer sequences used were ARv7: forward: TGA AGCAGGGATGACTCTGG, reverse: TCAGCCTTTCTT CAGGGTCTG, PSA: forward: GTCCCGGTTGTCTTC CTCAC, reverse: CTCCCACAATCCGAGACAGG, SKP2: forward: GGAAGGGAGTCCCATGAAA, reverse: GCT GAAGAGCAAAGGGAGTG, and GAPDH: forward: CTG GGCTACACT GAGCACC, reverse: AAGTGGTCGTTG AGGGCAATG. All assays were performed in triplicate. Data are presented as the fold change in gene expression relative to the control sample.

Luciferase assay

SKP2 promotor sequence (2000 bp upstream of transcription starting site) was cloned onto the pGL3 vector and co-transfected with Renilla plasmid into HEK293T cells, Luciferase activity was measured using the Dual-Luciferase Reporter Kit (Promega, Germany).

Annexin V/PI staining

After the desired infections and drug treatments, cells were stained with an Annexin V-FITC Apoptosis Detection Kit (BD Biosciences, CA, USA) according to the manufacturer's protocol and analyzed on a flow cytometer.

Senescence-associated-β-galactosidase activity assay

Senescence-associated-β-galactosidase (SA-β-gal) activity was detected using a Senescence β-Galactosidase Staining Kit (Beyotime, China) according to the manufacturer's instructions. In brief, cells were washed with PBS and then fixed for 10–15 min at room temperature with 1 ml of a fixative solution. After being washed, the cells were incubated overnight with the staining solution at 37 °C. Finally, the cells were observed under a microscope at a magnification of 200× to monitor the development of blue color. For quantification, at least 50 cells were counted for each field.

EdU (5-ethynyl-2′-deoxyuridine) assay

EdU assays were performed using a BeyoClick™ EdU-488 kit (Beyotime, China) according to the manufacturer's instructions. Basically, the cell culture medium was first mixed with an equal volume of 2× EdU working solution to a final concentration of 10 μM, and then the cells were incubated for another 2 h at 37 °C. After EdU labeling, the medium was removed and the cells

were fixed for 15 min at room temperature with 1 ml of a fixative solution. After washing and cell permeabilization, a Click Reaction Buffer was made and incubated with cells for 30 min at room temperature in the dark. Finally, cells were treated with DAPI for 2 min, and images were acquired by an Olympus FV1000 confocal laser microscope (×40 magnification). For quantification, at least 100 cells were counted for each field.

Chromatin immunoprecipitation (ChIP)-qPCR assay

ChIP assays were conducted using the ChIP Assay kit (P2078, Beyotime, China) according to the manufacturer's instructions. Chromatin samples were immunoprecipitated with antibodies against ARv7 (CST, 19672) or a negative control rabbit IgG antibody (CST). After the purification of DNA, gene promoter-specific sequences were amplified by qRT-PCR with designed primers (primer sequences are sense: GAGCAGCTCTGCAGT TAATGC, antisense: TATTAAGAGGGTCCATTTCAT GCT). Data are presented as the mean of three independent experiments (± SD), and the ChIP efficiency of certain binding sites was measured using the percentage of chipped DNA against the input.

Colony formation assay

After the desired virus infection and drug treatment, cells were seeded in six-well plates for 14 days with medium refreshment every 3 days. Then, the cells were fixed with 10% formalin and stained with 0.05% crystal violet. Quantifications of the clones were based on the mean values of at least three independent wells per condition.

Statistical analyses

The level of significance indicated by P values was calculated using standard two-sided Student's t-tests. $P < 0.05$ was considered statistically significant.

Abbreviations

ADT	Androgen deprivation therapy
AI	Androgen independent
AIS	ADT-induced senescence
AR	Androgen receptor
AR-FL	AR-full length
ARvs	Androgen receptor splicing variants
ARv7	Androgen receptor splicing variant 7
CHX	Cycloheximide
ChIP	Chromatin immunoprecipitation
CRPC	Castration-resistant prostate cancer
CSS	Charcoal-stripped serum
EMT	Epithelial-to-mesenchymal transition
ENZ	Enzalutamide
FDA	Food and Drug Administration
GSEA	Gene set enrichment analysis
KD	Knockdown
MTT	Methyl thiazolyl tetrazolium
OE	Overexpression
WB	Western blot
PCa	Prostate cancer
PSA	Prostate specific antigen
SASP	Senescence-associated secretory phenotype
SKP2	S-phase kinase-associated protein 2
SKP2i	SKP2 inhibitor
TIS	Treatment-induced senescence

Supplementary Information

The online version contains supplementary material available at https://doi.org/10.1186/s12915-025-02172-4.

Additional file 1: Original western blotting images.

Acknowledgements

We thank all the members of the Dr. Liankun Sun's laboratory for their comments and suggestions during the development of this manuscript.

Author's contributions

C.S. and J.K. designed the study. D.Z., H.L., T.Y., and X.L. performed experiments. C.S. and H.L. analyzed the data. C.S. and D.Z. wrote the manuscript with input from all authors. J.K. oversaw the project. All authors read and approved the final manuscript.

Funding

This work was supported by the National Natural Science Foundation of China (82373127), the Science and Technology Development Project Foundation of Jilin Province (20230101141JC), and the Jilin University Bethune Plan B Projects (2022B16 and 2024B37).

Data availability

The majority of data that support the findings of this study are included within the article and the remaining results, which are not displayed in the article, are available from the corresponding author upon reasonable request. Publicly available datasets used in the work included those from NCBI GEO accession numbers GSE99378 (ATAC-seq data of 22Rv1 cells, https://www.ncbi.nlm.nih.gov/geo/query/acc.cgi?acc=GSE99378) [47], GSE94013 (ChIP-seq for ARv7 and AR in 22Rv1 cells, https://www.ncbi.nlm.nih.gov/geo/query/acc.cgi?acc=GSE94013) [26], GDS3358 (longitudinal analysis of progression to androgen independence, https://www.ncbi.nlm.nih.gov/geo/query/acc.cgi?acc=GSE8702) [48], GSE35988 (*SKP2* expression in prostate tissues, https://www.ncbi.nlm.nih.gov/geo/query/acc.cgi?acc=GSE35988) [49], and GSE32269 (*SKP2* expression in prostate tissues, https://www.ncbi.nlm.nih.gov/geo/query/acc.cgi?acc=GSE32269) [50]. RNA-seq data in 22Rv-1 cells was from GSE277204 [29]. All data generated or analyzed during this study are included in this published article and its supplementary information files.

Declarations

Ethics approval and consent to participate

All the data generated using human samples were downloaded from publicly available database. This study does not involve the use of any human or animal samples or the participation of human subjects.

Consent for publication

Not applicable.

Competing interests

The authors declare that they have no competing interests.

Received: 3 January 2024 Accepted: 13 February 2025
Published online: 28 February 2025

References

1. Sung H, Ferlay J, Siegel RL, Laversanne M, Soerjomataram I, Jemal A, et al. Global cancer statistics 2020: GLOBOCAN estimates of incidence and mortality worldwide for 36 cancers in 185 countries. CA Cancer J Clin. 2021;71(3):209–49.

2. Tan MH, Li J, Xu HE, Melcher K, Yong EL. Androgen receptor: structure, role in prostate cancer and drug discovery. Acta Pharmacol Sin. 2015;36(1):3–23.
3. Perlmutter MA, Lepor H. Androgen deprivation therapy in the treatment of advanced prostate cancer. Rev Urol. 2007;9 Suppl 1(Suppl 1):S3–8.
4. Karantanos T, Corn PG, Thompson TC. Prostate cancer progression after androgen deprivation therapy: mechanisms of castrate resistance and novel therapeutic approaches. Oncogene. 2013;32(49):5501–11.
5. Graham L, Schweizer MT. Targeting persistent androgen receptor signaling in castration-resistant prostate cancer. Med Oncol. 2016;33(5):44.
6. Yuan X, Balk SP. Mechanisms mediating androgen receptor reactivation after castration. Urol Oncol. 2009;27(1):36–41.
7. Wadosky KM, Koochekpour S. Androgen receptor splice variants and prostate cancer: from bench to bedside. Oncotarget. 2017;8(11):18550–76.
8. Lu C, Luo J. Decoding the androgen receptor splice variants. Transl Androl Urol. 2013;2(3):178–86.
9. Xu J, Qiu Y. Role of androgen receptor splice variants in prostate cancer metastasis. Asian J Urol. 2016;3(4):177–84.
10. Zhang T, Karsh LI, Nissenblatt MJ, Canfield SE. Androgen receptor splice variant, AR-V7, as a biomarker of resistance to androgen axis-targeted therapies in advanced prostate cancer. Clin Genitourin Cancer. 2020;18(1):1–10.
11. Antonarakis ES, Lu C, Wang H, Luber B, Nakazawa M, Roeser JC, et al. AR-V7 and resistance to enzalutamide and abiraterone in prostate cancer. N Engl J Med. 2014;371(11):1028–38.
12. Hu R, Lu C, Mostaghel EA, Yegnasubramanian S, Gurel M, Tannahill C, et al. Distinct transcriptional programs mediated by the ligand-dependent full-length androgen receptor and its splice variants in castration-resistant prostate cancer. Cancer Res. 2012;72(14):3457–62.
13. Lu J, Lonergan PE, Nacusi LP, Wang L, Schmidt LJ, Sun Z, et al. The cistrome and gene signature of androgen receptor splice variants in castration resistant prostate cancer cells. J Urol. 2015;193(2):690–8.
14. He Y, Lu J, Ye Z, Hao S, Wang L, Kohli M, et al. Androgen receptor splice variants bind to constitutively open chromatin and promote abiraterone-resistant growth of prostate cancer. Nucleic Acids Res. 2018;46(4):1895–911.
15. Ewald JA, Desotelle JA, Church DR, Yang B, Huang W, Laurila TA, et al. Androgen deprivation induces senescence characteristics in prostate cancer cells in vitro and in vivo. Prostate. 2013;73(4):337–45.
16. Kawata H, Kamiakito T, Nakaya T, Komatsubara M, Komatsu K, Morita T, et al. Stimulation of cellular senescent processes, including secretory phenotypes and anti-oxidant responses, after androgen deprivation therapy in human prostate cancer. J Steroid Biochem Mol Biol. 2017;165(Pt B):219–27.
17. Huang W, Hickson LJ, Eirin A, Kirkland JL, Lerman LO. Cellular senescence: the good, the bad and the unknown. Nat Rev Nephrol. 2022;18(10):611–27.
18. Abbastabar M, Kheyrollah M, Azizian K, Bagherlou N, Tehrani SS, Maniati M, et al. Multiple functions of p27 in cell cycle, apoptosis, epigenetic modification and transcriptional regulation for the control of cell growth: a double-edged sword protein. DNA Repair (Amst). 2018;69:63–72.
19. Lin HP, Lin CY, Huo C, Hsiao PH, Su LC, Jiang SS, et al. Caffeic acid phenethyl ester induced cell cycle arrest and growth inhibition in androgen-independent prostate cancer cells via regulation of Skp2, p53, p21Cip1 and p27Kip1. Oncotarget. 2015;6(9):6684–707.
20. Kokontis JM, Lin HP, Jiang SS, Lin CY, Fukuchi J, Hiipakka RA, et al. Androgen suppresses the proliferation of androgen receptor-positive castration-resistant prostate cancer cells via inhibition of Cdk2, CyclinA, and Skp2. PLoS One. 2014;9(10): e109170.
21. Taylor W, Mathias A, Ali A, Ke H, Stoynev N, Shilkaitis A, et al. p27(Kip1) deficiency promotes prostate carcinogenesis but does not affect the efficacy of retinoids in suppressing the neoplastic process. BMC Cancer. 2010;10:541.
22. Chu IM, Hengst L, Slingerland JM. The Cdk inhibitor p27 in human cancer: prognostic potential and relevance to anticancer therapy. Nat Rev Cancer. 2008;8(4):253–67.
23. Coppé JP, Desprez PY, Krtolica A, Campisi J. The senescence-associated secretory phenotype: the dark side of tumor suppression. Annu Rev Pathol. 2010;5:99–118.
24. Carpenter V, Saleh T, Min Lee S, Murray G, Reed J, Souers A, et al. Androgen-deprivation induced senescence in prostate cancer cells is permissive for the development of castration-resistance but susceptible to senolytic therapy. Biochem Pharmacol. 2021;193: 114765.
25. Burton DG, Giribaldi MG, Munoz A, Halvorsen K, Patel A, Jorda M, et al. Androgen deprivation-induced senescence promotes outgrowth of androgen-refractory prostate cancer cells. PLoS One. 2013;8(6): e68003.
26. Cai L, Tsai YH, Wang P, Wang J, Li D, Fan H, et al. ZFX mediates non-canonical oncogenic functions of the androgen receptor splice variant 7 in castrate-resistant prostate cancer. Mol Cell. 2018;72(2):341–54.e6.
27. Yu B, Liu Y, Luo H, Fu J, Li Y, Shao C. Androgen receptor splicing variant 7 (ARV7) inhibits docetaxel sensitivity by inactivating the spindle assembly checkpoint. J Biol Chem. 2021;296: 100276.
28. Kallenbach J, Atri Roozbahani G, Heidari Horestani M, Baniahmad A. Distinct mechanisms mediating therapy-induced cellular senescence in prostate cancer. Cell Biosci. 2022;12(1):200.
29. Luo H, Liu Y, Li Y, Zhang C, Yu B, Shao C. Androgen receptor splicing variant 7 (ARv7) promotes DNA damage response in prostate cancer cells. FASEB J. 2022;36(9): e22495.
30. Gordon RR, Nelson PS. Cellular senescence and cancer chemotherapy resistance. Drug Resist Updat. 2012;15(1–2):123–31.
31. Smit MA, Peeper DS. Epithelial-mesenchymal transition and senescence: two cancer-related processes are crossing paths. Aging (Albany NY). 2010;2(10):735–41.
32. Milanovic M, Fan DNY, Belenki D, Däbritz JHM, Zhao Z, Yu Y, et al. Senescence-associated reprogramming promotes cancer stemness. Nature. 2018;553(7686):96–100.
33. Carpenter VJ, Patel BB, Autorino R, Smith SC, Gewirtz DA, Saleh T. Senescence and castration resistance in prostate cancer: a review of experimental evidence and clinical implications. Biochim Biophys Acta Rev Cancer. 2020;1874(2): 188424.
34. Yu P, Duan X, Cheng Y, Liu C, Chen Y, Liu W, et al. Androgen-independent LNCaP cells are a subline of LNCaP cells with a more aggressive phenotype and androgen suppresses their growth by inducing cell cycle arrest at the G1 phase. Int J Mol Med. 2017;40(5):1426–34.
35. Pernicová Z, Slabáková E, Kharaishvili G, Bouchal J, Král M, Kunická Z, et al. Androgen depletion induces senescence in prostate cancer cells through down-regulation of Skp2. Neoplasia. 2011;13(6):526–36.
36. Barakat DJ, Zhang J, Barberi T, Denmeade SR, Friedman AD, Paz-Priel I. CCAAT/enhancer binding protein β controls androgen-deprivation-induced senescence in prostate cancer cells. Oncogene. 2015;34(48):5912–22.
37. Grimmler M, Wang Y, Mund T, Cilensek Z, Keidel EM, Waddell MB, et al. Cdk-inhibitory activity and stability of p27Kip1 are directly regulated by oncogenic tyrosine kinases. Cell. 2007;128(2):269–80.
38. Cai Z, Moten A, Peng D, Hsu CC, Pan BS, Manne R, et al. The Skp2 pathway: a critical target for cancer therapy. Semin Cancer Biol. 2020;67(Pt 2):16–33.
39. Wang HH, Lee YN, Su CH, Shu KT, Liu WT, Hsieh CL, et al. S-phase kinase-associated protein-2 rejuvenates senescent endothelial progenitor cells and induces angiogenesis in vivo. Sci Rep. 2020;10(1):6646.
40. Fang Z, Zhang T, Dizeyi N, Chen S, Wang H, Swanson KD, et al. Androgen receptor enhances p27 degradation in prostate cancer cells through rapid and selective TORC2 activation. J Biol Chem. 2012;287(3):2090–8.
41. Li B, Lu W, Yang Q, Yu X, Matusik RJ, Chen Z. Skp2 regulates androgen receptor through ubiquitin-mediated degradation independent of Akt/mTOR pathways in prostate cancer. Prostate. 2014;74(4):421–32.
42. Rezaeian AH, Phan LM, Zhou X, Wei W, Inuzuka H. Pharmacological inhibition of the SKP2/p300 signaling axis restricts castration-resistant prostate cancer. Neoplasia. 2023;38: 100890.
43. Wüstmann N, Seitzer K, Humberg V, Vieler J, Grundmann N, Steinestel J, et al. Co-expression and clinical utility of AR-FL and AR splice variants AR-V3, AR-V7 and AR-V9 in prostate cancer. Biomark Res. 2023;11(1):37.
44. Roggero CM, Jin L, Cao S, Sonavane R, Kopplin NG, Ta HQ, et al. A detailed characterization of stepwise activation of the androgen receptor variant 7 in prostate cancer cells. Oncogene. 2021;40(6):1106–17.
45. Labaf M, Li M, Ting L, Karno B, Zhang S, Gao S, et al. Increased AR expression in castration-resistant prostate cancer rapidly induces AR signaling reprogramming with the collaboration of EZH2. Front Oncol. 2022;12: 1021845.
46. Wang J, Park KS, Yu X, Gong W, Earp HS, Wang GG, et al. A cryptic transactivation domain of EZH2 binds AR and AR's splice variant, promoting oncogene activation and tumorous transformation. Nucleic Acids Res. 2022;50(19):10929–46.

47. Chen Z, Wu D, Thomas-Ahner JM, Lu C, Zhao P, Zhang Q, et al. Diverse AR-V7 cistromes in castration-resistant prostate cancer are governed by HoxB13. Proc Natl Acad Sci U S A. 2018;115(26):6810–5.
48. D'Antonio JM, Ma C, Monzon FA, Pflug BR. Longitudinal analysis of androgen deprivation of prostate cancer cells identifies pathways to androgen independence. Prostate. 2008;68(7):698–714.
49. Grasso CS, Wu YM, Robinson DR, Cao X, Dhanasekaran SM, Khan AP, et al. The mutational landscape of lethal castration-resistant prostate cancer. Nature. 2012;487(7406):239–43.
50. Cai C, Wang H, He HH, Chen S, He L, Ma F, et al. ERG induces androgen receptor-mediated regulation of SOX9 in prostate cancer. J Clin Invest. 2013;123(3):1109–22.

Publisher's Note